HMG Advance Access published July 27, 2016

The progressive ankyloses protein ANK facilitates clathrin- and adaptor-mediated membrane traffic at the trans-Golgi network-to-endosome interface

Wenke Seifert[1], York Posor[2], Peter Schu[3], Gudrun Stenbeck[4], Stefan Mundlos[5,6,7], Sabine Klaassen[8,9], Peter Nürnberg[10], Volker Haucke[2], Uwe Kornak[5,6,7], Jirko Kühnisch[5,6,8*]

1 Institute of Vegetative Anatomy, Charité - Universitätsmedizin Berlin, Germany

2 Department of Molecular Pharmacology and Cell Biology, Leibniz-Institut für Molekulare Pharmakologie (FMP), Berlin, Germany

3 Department of Cellular Biochemistry, Universitätsmedizin Georg-August University, Göttingen, Germany

4 College of Health and Life Sciences, Brunel University, Uxbridge, United Kingdom

5 Institute for Medical and Human Genetics, Charité - Universitätsmedizin Berlin, Germany

6 FG Development and Disease, Max-Planck-Institute for Molecular Genetics, Berlin, Germany

7 Berlin-Brandenburg Center for Regenerative Therapies, Charité - Universitätsmedizin Berlin, Germany

8 Experimental and Clinical Research Center (ECRC) | Max-Delbrück-Centrum for Molecular Medicine (MDC), Charité - Universitätsmedizin Berlin, Berlin, Germany

9 Department of Pediatric Cardiology, Charité - Universitätsmedizin Berlin, Germany

10 Cologne Center for Genomics (CCG), University of Cologne, Germany

* Corresponding author:

jirko.kuehnisch@mdc-berlin.de
Dr. rer. nat. Jirko Kühnisch
Charité - University Medicine
Experimental and Clinical Research Center (ECRC) | Max-Delbrück-Centrum for Molecular Medicine (MDC)
Lindenberger Weg 80
13125 Berlin
Germany

Phone: +49(030)9406-3319
Fax: +49(030)9406-2536

Abstract

Dominant or recessive mutations in the progressive ankylosis gene *ANKH* have been linked with familial chondrocalcinosis (CCAL2), craniometaphyseal dysplasia (CMD), and mental retardation, deafness, ankylosis syndrome (MRDA). The function of the encoded membrane protein ANK in cellular compartments other than the plasma membrane is unknown. Here, we show that ANK localizes to the trans-Golgi network (TGN), clathrin-coated vesicles, and the plasma membrane. ANK functionally interacts with clathrin and clathrin associated adaptor protein (AP) complexes as loss of either protein causes ANK dispersion from the TGN to cytoplasmic endosome-like puncta. Consistent with its subcellular localization, loss of ANK results in reduced formation of tubular membrane carriers from the TGN, perinuclear accumulation of early endosomes, and impaired transferrin endocytosis. Our data indicate that clathrin/ AP-mediated cycling of ANK between the TGN, endosomes, and the cell surface regulates membrane traffic at the TGN/ endosomal interface. These findings suggest that dysfunction of Golgi-endosomal membrane traffic may contribute to *ANKH*-associated pathologies.

Introduction

Mutations within the *ANKH* gene cause three human monogenic disorders: dominant familial chondrocalcinosis (CCAL2, MIM 118600), dominant craniometaphyseal dysplasia (CMD, MIM 12300) and recessive mental retardation, deafness, ankylosis syndrome (MRDA) (1-3). All three conditions affect the musculoskeletal system in a distinct manner. CCAL2 is distinguished by formation of ectopic calcium pyrophosphate dihydrate (CPPD) deposits within articular cartilage and adjacent soft tissues (1, 4). In contrast, CMD patients develop a severe thickening of the skull (hyperostosis) and modelling defects of long bones (2, 5). Patients affected by the recessive MRDA syndrome, however, demonstrate a severe phenotype that is characterized by early onset ankylosis (bony fusion of joints), mild mental retardation, deafness, and hypophosphatemia (3). MRDA syndrome shows striking similarities to the mouse model *ank/ank*, which develops early onset ankylosis due to the homozygous *Ank* missense mutation E440X inducing a loss of protein function (3, 6, 7).

The mineralization pathology observed in *ank/ank* mice has led to the concept that changes of intra- and extracellular pyrophosphate (PPi) levels are causative for *ANKH*-associated pathologies and hence the protein is listed in databases as an inorganic pyrophosphate transporter (6, 8-12). In bone and cartilage biology, PPi is believed to negatively regulate biomineralization processes (8, 11, 13). Therefore, increased extracellular PPi levels and subsequent precipitation of CPPD crystals has been suggested to cause CCAL2 (9). On the other hand, lower extracellular PPi levels due to loss of ANK transport function have been attributed to pathological calcifications in CMD and *ank/ank* mice ankylosis (9). This model is supported by observations in *Xenopus oocytes,* in which ANK overexpression results in elevated PPi uptake, while introduction of CMD as well as *Ank* mutations abolishes PPi internalization (9). However, the incorporation of CCAL2 mutations did not affect PPi uptake kinetics (9).

ANK is a highly hydrophobic transmembrane protein that upon transient overexpression in Cos7 cells has been localized to the plasma membrane (PM) (6). Most topology models predict ANK with a variable number of 10 to 12 transmembrane domains (2, 6). During evolution ANK has been highly conserved as indicated by 82 % homology between human and zebrafish on protein level (2, 14). Strikingly, ANK shares no homology with any other protein or protein domain. The expression of ANK is not restricted to musculoskeletal tissues such as cartilage and bone. Abundant ANK levels are also detected in brain, heart, liver, muscle, and skin (6, 15). The ubiquitous presence of ANK in soft tissues suggests that besides its putative role as PPi transport protein ANK may fulfil hitherto unknown functions in cell physiology.

To explore these alternative functions, we here characterized the ANK protein at the biochemical and cell biological levels. We show that endogenous ANK localizes to the late secretory/ endosomal pathway with abundant levels in the trans-Golgi network (TGN), within clathrin-coated vesicles, and at the PM. We further show that the proper localization of ANK depends on clathrin and on the TGN/ endosome localized clathrin adaptor-protein complex AP1, a known regulator of TGN/ endosomal sorting. Moreover, we demonstrate that loss of ANK is associated with defects in the formation of secretory carriers from the TGN and with endosomal dysfunction. ANK-depleted cells display a perinuclear accumulation of EEA1- and transferrin (Tf) positive early endosomes, resulting in reduced Tf internalization. Collectively, these data suggest that dysfunction of Golgi-endosomal membrane traffic due to mutation or loss of ANK may contribute to *ANKH*-associated pathologies.

Results

ANK localizes to the TGN in fibroblasts

To obtain insights into the subcellular localization of ANK (human protein) we used antibodies specifically recognizing a C-terminal peptide within native ANK. Using these antibodies, endogenous ANK protein was localized to the perinuclear area in human fibroblasts, A549, and monkey Cos7 cells (Fig.1A, Fig.S1A). Counterstaining for different marker proteins of the secretory pathway such as endoplasmic reticulum to Golgi intermediate compartment 53 kDa protein (ERGIC-53), Golgi matrix protein 130 (GM130), trans-Golgi network protein 46 (TGN46), and the clathrin adaptor-protein complex AP1-γ1 (γ1-adaptin subunit of AP1) indicated that endogenous ANK is highly enriched at the Golgi complex and in post-Golgi vesicular carriers (Fig.1A see intensity plots), with the highest levels seen at the TGN. The Golgi localization of ANK was corroborated by transient overexpression of an ANK-GFP fusion protein (N-terminal tag) in HeLa cells (Fig.1B, white asterisk indicates non-transfected cell). Similarly, transient overexpression of Xpress-ANK in HeLa as well as A549 cells and subsequent detection of the N-terminal Xpress-tag also showed strong perinuclear ANK signals that colocalized partially with GM130 (Fig.S1B, see Fig.S1C for fusion protein stability). Non-transfected HeLa cells (Fig.S1B, white asterisk) and transfection of empty pcDNA4 vector did not produce Golgi staining indicating specificity of the Xpress antibody. In primary *ank/ank* mouse adult fibroblasts (MAF) we validated ANK antibody specificity (Fig.S1D). Consistent with the data from human cells, MAF isolated from wild-type (wt) animals showed abundant Ank (murine protein) immunoreactivity in the perinuclear area, where it overlapped extensively with the TGN marker protein AP1-γ1. By contrast, no Ank immunoreactivity above background was detected in *ank/ank* fibroblasts. The Golgi localization of Ank was further confirmed by biochemical subcellular fractionation experiments of tissue extracts. Ank was abundant in fractions of highly enriched Golgi membranes isolated from rat liver (Fig.1C) along with the Golgi marker proteins Golgi

SNARE 28 (GS28) and AP1-γ1. Finally, the distribution of Ank in linear sucrose gradients strongly overlapped with that of TGN/ endosome localized proteins such as AP1-γ1 and Rab4A (Fig.S1E). These results indicate that endogenous ANK is concentrated at the TGN and in post-Golgi vesicular carriers that may correspond to clathrin/AP1-derived vesicles (see further below).

ANK is concentrated in clathrin-coated vesicles and cycles between the PM and intracellular pools

Earlier reports studying ANK subcellular distribution had suggested overexpressed ANK to be present at the cell surface of Cos7 cells (6). Consistent with these findings, 3D-confocal imaging (z-stacking) of transfected HeLa cells showed a fraction of ANK at the PM [2] and within PM ruffles [3], in addition to a major ANK pool accumulating at the TGN [1] (Fig.1D). These data suggest that ANK may cycle between the TGN and the cell surface. To corroborate this hypothesis, we carried out cell surface biotinylation experiments detecting endogenous ANK in human fibroblasts. As expected, ANK partitioned between the non-biotinylated intracellular (CL) and the biotinylated PM fraction (CS) (Fig.1E). Subcellular accumulation of transiently transfected ANK-GFP at the PM and in perinuclear Golgi vesicles was similarly proven by live imaging experiments in ROS cells (Fig.S2A-B). In addition, fluorescence bleaching demonstrated recovery of ANK-GFP at the PM within 120 seconds. However, the Golgi ANK-GFP fluorescence did not recover within 120 seconds suggesting fast ANK transport from the Golgi towards the PM. In addition, we observed fusion and separation of ANK-GFP vesicles with dextran-containing endosomes (Fig.S2C) supporting the idea that ANK cycles between the TGN and PM.

Membrane traffic between the PM and the TGN involves, among other molecular pathways, clathrin-dependent mechanisms and ANK localization in cell lines indicated its transport by AP1/ clathrin. Next, we analyzed a possible involvement of clathrin in ANK

sorting using tissue extracts. Indeed, ANK was detected in clathrin-coated vesicles (CCV) isolated from bovine brain, along with clathrin and AP2 α-adaptin (a subunit of the clathrin adaptor AP2) (Fig.1F). The presence of ANK in CCVs was further validated in CCV preparations from control and *ank/ank* mouse brain; with absence of an Ank signal in *ank/ank* samples (Fig.1F). These results suggest that ANK cycles between the TGN and the PM, likely via AP1 and AP2 CCV. Thus, we decided to investigate the mechanism of ANK sorting in vesicular protein transport as well as the possible function of ANK within the TGN/ endosomal system in more detail.

Intracellular ANK trafficking involves clathrin/ AP-dependent sorting

To obtain insights into the mechanism of ANK sorting, we examined the primary sequence for protein domains or peptide motifs that mediate interaction with the sorting machinery. We noticed a cluster of acidic residues within the C-terminal cytoplasmic domain (E460-E492) of ANK (Fig.S3). The N-terminal cytoplasmic domain of ANK harbors tyrosine based YxxΦ motifs. Acidic cluster and the YxxΦ motifs are recognized by the μ-adaptin subunits of AP complexes, which is in line with ANK transport via CCV. Cluster of acidic residues are also bound by phosphofurin acidic cluster sorting protein 1 (PACS-1), which regulates endosomal protein sorting, while its function in CCV mediated transport is being debated (16, 17). Clathrin-mediated endocytosis of transmembrane cargo from the PM via CCV requires the AP2 complex, whereas AP1 facilitates protein traffic via CCV between the TGN and endosomes (17, 18). To test a possible role of the ANK N- and C-terminal domains for its subcellular sorting, we generated chimeric fusion proteins of both ANK domains. In one construct, we replaced the N-terminal domain of the TfR with that of ANK (residues M1-F76 fused to TfR amino acids N55-F760). In a second construct, we generated a chimera between the C-terminal domain of ANK (R453-E492) and the CD8 alpha chain (CD8 amino acids M1-C206), a protein lacking endocytic sorting motifs (Fig.2A). Co-overexpressed full

length TfR-GFP and ANK-wt colocalized at the perinuclear area corresponding to the TGN/ recycling endosomal interface (Fig.2B). By contrast, neither ANK-TfR nor CD8a-ANK colocalized with TfR-GFP in the perinuclear area (Fig.2C). These data suggest that neither the N- nor the C-terminal cytoplasmic domains of ANK on their own are sufficient to mediate proper ANK sorting, although it is possible that the putative AP binding motifs identified within these domains contribute to ANK sorting and function.

To unravel the mechanisms for ANK sorting, we focused on the clathrin sorting machinery. We capitalized on the observation that ANK is highly enriched in CCVs (Fig.1F), suggesting that clathrin and clathrin-recruiting APs may lie at the heart of the machinery for ANK sorting. We tested this hypothesis by focusing on AP1, a TGN/ endosome adaptor complex mediating clathrin-dependent sorting of YxxØ- and dileucine motif-containing cargo between the TGN and endosomes (19). First, we analyzed the localization of Ank in mouse embryonic fibroblasts (MEF) derived from AP1-µ1A knockout mice. Strikingly, Ank failed to accumulate at the TGN and instead displayed a dispersed localization in µ1A-/- MEFs, akin to the phenotype observed for the mannose 6-phosphate receptor (MPR46), which recycles between the PM, endosomes and the TGN and is a known AP1 cargo (20). This effect was caused by loss of AP1 function as the normal TGN localization of Ank was restored in a rescued cell line (µ1A-/-::µ1A), in which µ1A is re-expressed (Fig.2D). As a second independent approach we studied HeLa cells depleted of the γ1-subunit of the adaptor protein complex 1 (protein AP1-γ1, gene AP1G1) by specific siRNAs. Knock-down (KD) of AP1G1/ AP1-γ1 in HeLa cells phenocopied loss of AP1-µ1A as evidenced by the cytoplasmic dispersion of ANK from the perinuclear TGN area (Fig.2E). Similar phenotypes were observed upon KD of clathrin heavy chain (CHC), PACS-1, a sorting adaptor for acidic motifs (21), and the endocytic clathrin adaptor µ2-subunit of the AP2 complex (protein AP2-µ2, gene AP2M1) (Fig. 2E-F). These results are consistent with the cycling of ANK between

the TGN, endosomes, and the cell surface via clathrin/ AP-dependent sorting mechanisms and are reminiscent of the behavior of recycling membrane proteins such as MPR46/300 (20, 22).

ANK is a post-Golgi protein cycling between the TGN and PM

To further explore the relationship between ANK localization and subcellular compartment integrity, we treated HeLa cells with nocodazole, monensin, or brefeldin A (BFA), drugs that perturb Golgi structure and function (23). Microtubule depolymerization by nocodazole led to Golgi disassembly (24) and to the accumulation of ANK in AP1-γ1-positive membrane puncta (Fig.3A), suggesting that ANK traffics to or from the TGN via a microtubule-based mechanism. Application of the cationic ionophore monensin, a drug that disrupts Golgi pH-gradients and thereby blocks intra-Golgi transport (23, 25), caused ANK to localize to the Golgi and to cytoplasmic TGN-derived vesicles, consistent with the data indicating that a fraction of ANK is present in post-Golgi compartments. Finally, application of BFA, an inhibitor of Arf-mediated recruitment of coat proteins (including AP1) to Golgi membranes (23, 26, 27), leading to fusion of the ER with the Golgi and of the TGN with endosomes caused a partial segregation of ANK from TGN46-positive TGN fragments. In line with ANK being a TGN/ endosome enriched protein, no colocalization with ERGIC53-positive ER exit sites was observed. This experimental setup further proves that perinuclear ANK enrichment does not arise from ER derived membranes.

Next, we blocked clathrin-mediated transport with the dynamin inhibitor dynasore in HeLa cells and followed ANK-GFP distribution. Steady-state immunostaining of TfR, which is exclusively sorted by clathrin-mediated mechanisms, showed strong overlap with ANK-GFP at the perinuclear region (Fig.3B). Treatment with dynasore redistributed TfR into cytoplasmic vesicles. This is consistent with the silencing of post-Golgi and endosomal membrane transport by dynasore (28). With dynasore treatment the ANK signal remained enriched at the perinuclear region. Incubation of ANK-GFP transfected cells with

chloroquine, a lysosomotropic agent preventing endosomal acidification (29), induced a striking accumulation of ANK at the PM and loss of the perinuclear signal (Fig.3B, see line scans). In parallel, TfR redistributed into cytoplasmic vesicles. Chloroquine treatment does not block secretory protein transport, suggesting that the ANK accumulation at the PM results from blunted ANK internalization. We conclude that ANK is sorted to and from the TGN via AP1/ microtubule-based mechanisms, exits the TGN via TGN46 positive carriers, is internalized at the PM via acidified endosomes, and does not redistribute to the ER or to ER exit sites under conditions that disrupt Golgi integrity.

ANK regulates tubular carrier formation at the TGN but is not required for Golgi integrity

To investigate the subcellular function of ANK we first assessed its expression in different cell lines. Highest ANK mRNA levels were found in HeLa, Hek293, TC28, and SAOS-2 cells (Fig.S4A). Based on these data we evaluated three different siRNAs for their efficiency to ablate ANK mRNA and protein expression in HeLa cells. siRNAs ANK#1 and ANK#3 each resulted in ANK depletion by approximately 95 % compared to controls (Fig.S4B). None of these siRNAs altered mRNA expression levels of ectonucleotide pyrophosphatase/ phosphodiesterase 1 (ENPP1) or AP1G1 used as controls. Efficient ablation of ANK protein expression was further corroborated by immunostaining and Western blot analysis (Fig.S5A-B).

The Golgi apparatus is formed by individual cisternae that are organized in a cis-trans orientation and maintained by continuous membrane transport (30). Given the accumulation of ANK at the TGN, we analyzed the consequences of ANK ablation on Golgi cisternal organization. After ANK KD, the Golgi structure was not altered as assessed by immunostaining with AP1-γ1 as well as TGN46 (Fig.S5C). We further tested the partitioning of cis- and trans-Golgi markers such as GM130 vs. TGN46 and GS28 vs. RAB6. We detected

no difference in the cis-trans distribution of Golgi marker proteins (Fig.S5D). In addition, the Golgi ultrastructure appeared unaffected after KD of ANK (Fig.S5E). These observations indicate that ANK is not required for the structural integrity or polarity of the Golgi complex.

A major function of the TGN is the formation of vesiculo-tubular membrane carriers that traffic secretory cargo towards the PM. Based on the above experiments and on the steady-state partitioning between the TGN, endosomes, and the PM, we hypothesized that ANK may exit the TGN in tubular membrane carriers *en route* to the cell surface. To explore this hypothesis further, we treated HeLa cells with a short pulse of BFA to induce Golgi tubulation (26, 31). Under these conditions, ANK colocalized with TGN46 in Golgi-derived membrane tubules (Fig.4A). Next, we assessed BFA-induced formation of Golgi-derived membrane tubules directed towards the ER or to the PM and endosomes using RAB6 or TGN46 as markers, respectively (25, 32). Loss of ANK led to a severe reduction in the number and length of both, RAB6- and TGN46-positive membrane tubules (Fig.4B, C). These data suggest that ANK, although dispensable for Golgi integrity, affects the formation of TGN-derived membrane transport tubules.

ANK is required for endosomal function and endocytosis

At the TGN/ recycling endosome boundary secretory and endocytic membrane traffic intersect. For example, clathrin/ AP1 is involved in membrane traffic between endosomes and the TGN, in polarized sorting to the basolateral PM via recycling endosomes, and in synaptic vesicle recycling (30, 33). Furthermore, internalized TfR is stored in recycling endosomes via retrograde traffic from EEA1-positive early endosomes (34, 35). Given the functional defects at the level of the TGN in ANK-depleted cells and based on the partitioning of ANK between the TGN, endosomes, and the PM we speculated that loss of ANK may also lead to defects in the endosomal system. To test this, we analyzed the distribution of early endosomes as well as TfR endocytosis in cells depleted by ANK with specific siRNAs. We first visualized the

localization of early endosomes with pulsed (6 min) Tf endocytosis by confocal microscopy. All three ANK siRNAs induced a perinuclear accumulation of endocytosed Tf, while in controls internalized Tf localized to peripheral early endosomes homogeneously distributed throughout the cytosol (Fig.5A). The perinuclear concentration of early endosomes was further corroborated by analyzing the distribution of the early endosomal marker protein EEA1 (Fig. 5B). This phenotype is reminiscent to that induced by KD of KIF16B, an anterograde motor that facilitates the peripheral dispersion of early endosomes (36). Further quantitative analyses revealed significantly delayed Tf endocytosis kinetics in ANK-depleted HeLa cells (Fig.5C), suggesting that ANK is critical for endosome distribution and function.

Following internalization, TfR is recycled back to the PM via a fast (out of early endosomes) and a slow (out of recycling endosomes) routes (30), which depend in part on endosomal distribution and their transport dynamics. Consistent with a critical role for ANK in endosome function, Tf recycling appeared delayed in ANK-depleted cells (Fig.5D). This may be a consequence of the altered distribution of early endosomes within ANK-depleted cells as both control and ANK KD cells were equally competent in forming endosomal membrane tubules when treated with a short pulse of BFA (Fig.5E). These observations are consistent with a model whereby ANK, directly or indirectly, regulates the partitioning of TfR/Tf between perinuclear recycling endosomes and the cell surface. To probe such partitioning, we used imaging of pHluorin-tagged TfR in control vs. ANK KD cells (37). As expected, ANK-depleted cells showed mildly elevated TfR surface levels at steady-state or upon a Tf pulse (Fig.5F), consistent with a reduced rate of TfR endocytosis. Accordingly, ablation of ANK caused slightly elevated TfR levels in non-acidic compartments (i.e. CCVs) upon TfR/Tf endocytosis. Collectively, our observations indicate that ANK is critical for proper endosomal function and thus endocytic pathways.

Discussion

This study provides insights into the subcellular localization and function of the ankylosis protein ANK a putative PM transporter and regulator of intracellular PPi levels. Our data indicate that ANK localizes to the TGN, CCV, and the PM and regulates TGN as well as endosomal membrane traffic. Specifically, we demonstrate that loss of ANK is associated with perinuclear clustering of early endosomes and corresponding defects in TfR/Tf endocytosis and recycling.

The most striking effect of ANK-deficiency on subcellular compartments is the perinuclear accumulation of early endosomes. To our knowledge, perinuclear concentration of endosomes after KD of a putative channel protein has not been described in the literature. However, comparable phenotypes have been described for mutations or the depletion of several proteins: the endosome-associated kinesin motor KIF16B, the endosomal regulators annexin A2, Alix, and the brefeldin A-inhibited guanine nucleotide-exchange protein 2 (BIG2) (36, 38-40). Annexin A2 is a calcium and lipid-binding protein and loss of annexin A2 induces perinuclear endosome clustering, however without apparent changes in TfR/Tf uptake and recycling (38). Recently, annexin A2 dependent actin nucleation at early endosomes has been shown to regulate endosome maturation and remodeling (41). Loss of Alix, a component of the ESCRT based machinery for multivesicular body formation in late endosomes, likewise is associated with a perinuclear accumulation of internalized TfR/Tf and concomitant changes in the organization of the actin cytoskeleton (39). In contrast, the ARF-GEF BIG2, a factor that regulates TGN membrane association of AP1 via Arf1 (42), facilitates TfR/Tf recycling by modulating the distribution of recycling endosomes (40). Lastly, KD of KIF16B, a FYVE-domain containing kinesin motor on early endosomes, causes perinuclear early endosome concentration and altered rates of recycling vs. degradation of internalized proteins (36). Although this heterogeneous group of proteins has not been associated with ANK, they all affect endosome morphology or distribution either by

controlling the cytoskeleton or by recruitment and activation of factors required for membrane traffic. ANK may directly or indirectly affect such processes, although the precise underlying mechanisms remain to be determined. Given the low abundance of ANK in endosomal compartments compared to the TGN, we favor a model according to which the effects of ANK on endosomes are secondary to altered trafficking at the level of the TGN. This idea is further supported by the observation that the subcellular localization of ANK itself is controlled by CCV and clathrin-associated adaptors such as AP1, AP2, and PACS-1.

Transmembrane proteins, in particular channels/ transporters, may regulate membrane traffic by a variety of mechanisms including the control of ion homeostasis (43-45) and the luminal pH (46, 47). Within the secretory pathway, the pH declines continuously from the ER (pH 7.2) to the TGN (pH 6) and within the endocytic pathway from early endosomes (pH 6.3) to recycling endosomes (pH 6.5), and finally late endosomes and lysosomes (pH 5.5) (46). Luminal pH is controlled by vacuolar proton pumps (vATPases), calcium ATPases, sodium/ proton exchangers, and proton/ chloride exchangers. Changes in luminal organelle pH are required for membrane fusion, ligand-receptor dissociation, cargo maturation, or actin cytoskeleton dynamics (46). ANK localizes to the PM and to the TGN, initiation sites for CCV formation by AP2 and AP1 respectively. Interestingly, knock-down of the endosome/ TGN-localized subunit a2 of the H^+-ATPase results in a similar perinuclear shift of endosomes (unpublished observation). It is thus possible that ANK regulates the luminal pH in the TGN and endosomes. Indeed, increased TfR levels at the PM and reduced Tf uptake upon loss of ANK are reminiscent of findings in cells deficient for the proton/ chloride exchanger ClC-4 (45). A role in vesicular acidification has also been established for other endosomal members of the ClC family (46). Such a pH-regulatory function of ANK could either be a direct consequence of its ion transport activity or could be caused indirectly, e.g. by controlling energy supply required for ion pumping. The latter idea is consistent with the

proposed function of ANK as a PPi transport protein (6, 9) and with the observation that PPi serves as a high energy compound sufficient for TGN acidification in rat liver (48).

A surprising observation of our study is the enrichment of ANK at the PM upon chloroquine treatment. Chloroquine is a lysosomotropic drug that accumulates in acidic organelles, such as endosomes and lysosomes, where it raises the pH resulting in altered fusion of membrane vesicles and degradation of cargo molecules (29, 49). Trapping of ANK at the PM in the presence of chloroquine supports our finding that ANK permanently cycles between the TGN and PM. A regulatory role of ANK for endolysosomal acidification would be consistent with its subcellular localization and the observed endosomal trafficking defects after ANK ablation. Of note, disruption of endosomal acidification with chloroquine has been linked with sustained WNT signaling (50) and increased cell surface levels of bone morphogenetic protein receptor type-II (BMPR-II) (51). Both, WNT and BMP pathways are key mechanisms that regulate chondrocyte and osteoblast differentiation and function (52, 53). Increased levels of Wnt5a after loss of ANK control canonical WNT signaling and have been associated with the maintenance of a chondrocyte differentiation phenotype *in vitro* (54). Thus, analyzing possible molecular mechanisms of ANK in endosomal acidification is a worthwhile approach to provide novel insights into the molecular pathomechanisms of CCAL2, CMD, and MRDA.

Whether and how ANK mutations disturb the mechanisms by which ANK is intracellularly sorted is unknown. However, it is interesting to note that the *ANKH*-associated diseases CCAL2, CMD, and MRDA syndrome have been linked to distinct mutation hotspots (Fig.S3) (1-3). In the case of CCAL2, mutations are found in close proximity of YxxΦ motifs or acidic cluster signals that may contribute to ANK sorting *in vivo*. Relating these mutations to the intracellular distribution and function of ANK based on the findings reported here remains an interesting subject for future studies.

In summary, our work identifies ANK as a transmembrane protein that cycles between the PM, endosomes, and the TGN via a mechanism that depends on the CCV forming clathrin-adaptor-protein complexes AP1 and AP2. Loss of ANK results in defective tubular membrane carrier formation at the TGN, the perinuclear accumulation of early endosomes, and in reduced TfR/Tf endocytosis. These findings extend the function of ANK as PM transporter to a regulator of TGN/ endosome membrane dynamics. Our work thus provides the basis for an improved understanding of the function of ANK and the pathomechanisms of *ANKH*-related disorders.

Materials and methods

Materials and antibodies

All materials were purchased from Sigma unless otherwise stated. A polyclonal rabbit anti-peptide antibody was raised by repeated immunization of the KLH-coupled C-terminal ANK peptide (VTDIVEMREENE-COOH). Anti-ANK antibody was purified by anti-peptide affinity purification from rabbit serum and used for immunofluorescence and Western blot analyses to detect endogenous protein. A second anti-ANK (generated in goat) antibody used to detect endogenous protein by Western blot was a kind gift from Jeffrey Winkles (American Red Cross, Rockville, Maryland) (15). This antibody was used for immunodetection of ANK in rat liver Golgi fractions. The following commercial antibodies were used in this study: α-adaptin (BD Bioscience), γ-adaptin (AP1-γ1) (BD), Clathrin heavy chain (BD Bioscience), EEA1 (BD Bioscience), ERGIC-53 (Alexis), FLAG (Sigma), GFP (Roche), GM130 (BD Bioscience), GS28 (BD Bioscience), Rab4a (Santa Cruz), RAB6 (Santa Cruz), PDI (Stressgene), TGN46 (Serotech), TfR (zymed) and Xpress (Invitrogen). Secondary antibodies were purchased for Western blot from Cell Signaling and for immunofluorescence detection from Molecular Probes. Polyclonal sheep antibody to GM130 was kindly provided by Francis Barr (University of Liverpool). 4',6-diamidino-2-phenylindole (DAPI, Invitrogen) was used for nuclear staining. Restriction enzymes were purchased from NEB.

μ1A-/- and μ1A-/-:μ1A fibroblasts were from Peter Schu (University of Göttingen). Golgi enriched rat liver fractions were kindly provided by John Caldwell (University of Colorado) (55). *ank/ank* mice were maintained under standard conditions. All animal experimental procedures were approved by the 'Landesamt für Gesundheits und Soziales (LaGeSo), Berlin, Germany.

Plasmid design

The following mammalian expression vectors were used in this study pcDNA4_Ank_wt, pFlag-CMV-5_Ank_wt, pEGFPC1_Ank_wt, pcDNA4_Ank_TfR, pcDNA4_CD8_Ank, and pC1_pHluorin-TfR. The murine *Ank* gene was used for vector cloning as it is highly homologues to human *ANKH*. For the pcDNA4_Ank_wt construct the murine *Ank* sequence (ENSMUSG00000022265) was amplified by PCR with flanking BamH1 restriction sites and subsequently inserted into the pcDNA4/HisMax vector (Invitrogen). For the pFlag-CMV-5_Ank_wt construct the murine *Ank* sequence was amplified by PCR with flanking BamH1 restriction sites and subsequently inserted into the pFlag-CMV-5 vector (Sigma). For the pEGFPC1_Ank_wt construct the murine *Ank* sequence was amplified by PCR with flanking BamH1 restriction sites and subsequently inserted into the pEGFPC1 vector. For the pcDNA4_Ank_TfR construct a fusion PCR product containing Ank M1-F76 and TfR N55-F760 with flanking BamH1 restriction sites was amplified by PCR and subsequently inserted into the pcDNA4/HisMax vector. For the pcDNA4_CD8_Ank construct a fusion PCR product containing the CD8alpha chain M1-C206 and Ank R453-E492 with flanking BamH1 restriction sites was amplified by PCR and subsequently inserted into the pcDNA4/HisMax vector. Superecliptic pC1_pHluorin-TfR was cloned by amplification of the human *TfR* (ENSG00000072274) coding sequence and subcloning into the BamHI restriction sites of pCI-pHluorin-cellubrevin (kindly provided by Richard Schlegel).

Cell culture and transient transfection

All cell lines were cultured at 37 °C, 5 % CO_2 in DMEM supplied with 5 % of fetal calf serum (FCS) and 2 mM ultraglutamine. Primary mouse and human fibroblast were grown at 37 °C and 5 % CO_2 in alpha-MEM complemented with 10 % FCS, 2 mM ultraglutamine, 100 µg/ml penicillin G, and 100 µg/ml streptomycin. Preparation of osteocytes were cultured as described elsewhere (56). Transfection of plasmid DNA was performed with jetPEI (Polyplus transfection) according to the manufacturer's protocol. Briefly, 3 µg plasmid DNA was

diluted in 100 µl sterile 0.9 % NaCl, mixed with an equal volume of a 6% (v/v) jetPEI dilution in sterile 0.9 % NaCl and incubated at room temperature for 20 min. The transfection mix was then added dropwise into the cell culture dish and left at least for 24 hours until subsequent analysis. *ank/ank* mouse fibroblasts were isolated from diaphragms by collagenase digest and subsequently cultured in fibroblast medium. Primary cell lines used in this study were of low passage number. To assess intracellular transport processes HeLa cells were treated with the microtubule-depolymerizing drug nocodazole (5 µM, 60 min), the cation ionophore monensin A (10 µM, 60 min) and the anterograde protein transport inhibitor brefeldin A (BFA) (5 µg/ml, 60 min). After transfection of HeLa cells with ANK-GFP endosomal transport was blocked either with the dynamin inhibitor dynasore (40 µM, 60 min) or the lysosomotropic agent chloroquine (200 µM, 60 min). After subsequent fixation, cells were immunostained and imaged with confocal microscopy.

SDS-PAGE and Western blot

For Western blot analysis, all samples were diluted in 1x SDS loading buffer and resolved by gel electrophoresis in Bis-Tris SDS polyacrylamide gels. Protein concentrations were determined when required, using the BCA protein assay kit (Pierce). After transfer on nitrocellulose membranes by tank blotting and blocking in 5% block milk, 0.2% NP-40 in 1xTBS, blots were incubated with the appropriate primary and secondary antibodies in 5% blocking milk and finally detected using ECL reaction (Amersham) and visualized on Super RX X-ray film (Fuji Film).

Immunofluorescence

For immunofluorescence detection of overexpressed and endogenous protein, cells were grown on glass coverslips (12 mm, Marienfeld), fixed with 4% (w/v) paraformaldehyde (PFA) in PBS; permeabilized in 1% (v/v) Triton X-100 in 3% (w/v) bovine serum albumine

(BSA) in PBS and blocked with 3% (w/v) BSA in PBS. Primary antibodies were applied in 3% BSA in PBS for 5 h at 4 °C, coverslips were washed in PBS, secondary antibodies and DAPI were applied in 3% BSA in PBS for 1 h at 4 °C, washed in PBS. Finally, coverslips were mounted on slides using Fluoromount-G (SouthernBiotech). Images were taken with a confocal microscope LSM510 (Zeiss). Images for subsequent evaluation were acquired under identical exposure conditions. Image analysis was performed with macros in AxioVision (Zeiss) under identical threshold conditions. Statistical significance was calculated with Student's t-test (two-sided, unpaired, homogenous variation).

Live Imaging

For live imaging, 10^5 cells were seeded in a 14 mm glass-bottomed dish (MatTek) and transfected with pEGFPC1_Ank_wt as described above. 48 h after transfection cells, immediately prior to imaging, cells were washed and transferred to prewarmed imaging medium (Opti-Prep medium (Invitrogen) supplemented with 0.5 % bovine serum albumin, 30 mM HEPES/NaOH pH 7.4 and 1 mM $CaCl_2$). Cells were then placed in a heated chamber at 37 °C and imaged with a Zeiss LSM510 microscope equipped with a 63x oil lens. For FRAP experiments, three section per cell recorded. After a short light pulse to bleach the area of interest, recovery of fluorescence was observed for the same section for up to 980 sec. For labelling of the lysosomal compartment, ROS 17/2.8 cells transfected with pEGFPC1_Ank_wt were grown in 14 mm glass-bottomed dish (MatTek) and incubated for 30 min with 130 µg/ml TRITC labelled dextran 10,000 (Invitrogen). Cells were imaged after removal of labelling medium and transfer into prewarmed imaging medium.

Sucrose gradient centrifugation

Separation of mouse liver postnuclear supernatants (PNS) in linear sucrose gradients was carried out at 4 °C and all solutions were complemented with protease inhibitor cocktail

(Roche). Briefly, freshly harvested liver was homogenized in a glass potter after adding 4 ml of 3 mM imidazole buffered 0.25 M sucrose solution per gram of fresh liver. PNS were obtained by centrifugation of the homogenate at 1000x g for 10 minutes. Linear sucrose gradients were prepared by using a gradient mixture device. PNS were carefully loaded on top of each gradient with a Pasteur pipette and centrifuged at 100.000x g for 2.5 hours in a SW32 swing out rotor. Fractions were obtained after centrifugation from a hole at the bottom of the centrifugation tube. Linearity of the gradient was assessed by measuring the refractive index of each fraction.

Cell surface biotinylation

Transient transfected or untreated living cells were labelled with EZ-Link Sulfo-NHS-LC-LC-Biotin Reagent (Pierce) for 30 minutes at 4 °C. Remaining labelling reagent was deactivated by washing with ice cold 100 mM glycine phosphate buffer pH 7.4. Cells were lysed in Tris buffer pH 7.1 supplemented with 1 % Triton X-100, complete proteinase inhibitor (Roche), 30 mM sodiumpyrophosphate, and 5 mM EDTA. Biotin labelled protein was separated with Streptavidin-agarose beads (Pierce). Following separation agarose beads were washed four times with lysis buffer. Both the supernatants as well as the bead fractions were dissolved in SDS sample buffer and subjected to SDS-PAGE followed by Western blot analysis.

Clathrin-coated vesicle preparation

Clathrin-coated vesicles from calf brain were isolated as described elsewhere (57). Clathrin-coated vesicles from mouse brain were prepared as described elsewhere (58).

RNAi treatment

Gene silencing in HeLa cells was performed by Interferin (Polyplus) transfection of siRNA (Ambion) according to manufacturer's instructions. The following siRNAs (Ambion) were

used in this study: scramble, ANK#1 (sense sequence 5´-3´ CACUGAUAGCUUAUAGUGAtt), ANK#2 (5´-3´ GGAUACUACAUUAUCAAUAtt); ANK#3 (CGUGCUAUGUCUACCGGAAtt); AP1G1 (ACCGAAUUAAGAAAGUGG); AP2M1 (GUGGAUGCCUUUCGGGUCAUU); CHC (AUCCAAUUCGAAGACCAA); PACS-1 (GCACGCAGAUUCCAAGAAAtt).

Quantitative PCR

Total RNA was isolated from cell cultures using peqGOLD TriFAST reagent (peqlab) according to the manufacturer's instructions. 1 µg isolated RNA was reverse transcribed using RevertAid H Minus First Strand cDNA Synthesis kit and random hexamer primers (Fermentas). Primer pairs for cDNA amplification were designed and sequences are available on request. mRNA levels were determined by quantitative PCR (qPCR) using 5x HotFirePol EvaGreen (Solis BioDyne) according to the manufacturer´s instructions. Each sample was analyzed as triplicate and amplified on an ABI PRISM7500 instrument (Applied Biosystems). Relative mRNA levels were quantified using the comparative Ct method (Smittgen und Livak). The different mRNA values were normalized against *GAPDH/Gapdh* mRNA.

Transferrin endocytosis and recycling

Analysis of transferrin (Tf-Alexa Fluor 555, Invitrogen) internalization was performed on siRNA-treated HeLa cells. Cells were seeded on glass coverslips. Prior to Tf application cells were starved in 5 mg/ml BSA in DMEM for 6 h. For Tf internalization, 5 µg/ml Tf-Alexa Fluor 555 (Invitrogen) in 5 mg/ml BSA in DMEM was prewarmed to 37 °C and directly added to the cells for the indicated time of length. For pulse-chase Tf trafficking cells were pulsed for 30 min with 5 µg/ml Tf-Alexa Fluor 555 (Invitrogen) in 5 mg/ml BSA in DMEM at 18 °C. The chase was initiated by shifting cells to 37 °C after washing twice with 5 mg/ml BSA in DMEM. Tf trafficking was terminated at indicated time points by fixing cells in 4%

PFA in PBS at 4 °C. Subsequently, coverslips were subjected to immunostaining, confocal imaging and image analysis.

Imaging of pHluorin-based transferrin receptor distribution to acidic vs. non-acidic vesicles

Characterization of acidic and non-acidic vesicles in HeLa cells was performed as described elsewhere (37). Briefly, HeLa cells treated with scramble and ANK#1 siRNA were transiently transfected with superecliptic pC1_pHluorin-TfR vector. Cells were seeded on cover slips that were for analysis placed in a perfusion flow chamber. Fluorescence was imaged with a spinning disc live cell imaging system, Ultra View ERS (Perkin-Elmer) including Zeiss Axiovert 200M. Imaging of the fluorescence occurred upon perfusion with different pH buffer conditions pH 7.4, 5.5 and 10. Fluorescence was measured with (5 µg/ml) and without Tf stimulation. Course of fluorescence intensity was evaluated with the slidebook (3i intelligent imaging innovations, USA) software package. Distribution of pHluorin-TfR in non-acidic CCV and at the PM was calculated from fluorescent intensities at individual pH values (pH 7.4 - PM + non-acidic CCV, pH 5.5 - non-acidic CCV, pH 10 PM + CCV + endosomes).

Acknowledgements

We wish to thank the Charité electron microscopy facility (P. Schrade and S. Bachmann) for excellent collaboration. Part of this work has been supported by grants SFB577/ A04 (PN and UK), DFG 802/3-2, /3-4 (PS), SFB958/ A01 (VH), and TRR186/ A08 (VH) from the German Research Funding Agency DFG.

Authors´ roles: Study design: WS, PN, VH, UK, JK. Performed research: WS, YP, PS, GS, JK. Analysed data: WS, JK. Critically reviewed manuscript: SM, SK, VH, UK. Wrote the manuscript: WS, JK. All authors read and approved the manuscript.

Conflict of interest

Authors have no competing interests to declare.

References

1 Pendleton, A., Johnson, M.D., Hughes, A., Gurley, K.A., Ho, A.M., Doherty, M., Dixey, J., Gillet, P., Loeuille, D., McGrath, R. *et al.* (2002) Mutations in ANKH cause chondrocalcinosis. *Am J Hum Genet*, **71**, 933-940.

2 Nurnberg, P., Thiele, H., Chandler, D., Hohne, W., Cunningham, M.L., Ritter, H., Leschik, G., Uhlmann, K., Mischung, C., Harrop, K. *et al.* (2001) Heterozygous mutations in ANKH, the human ortholog of the mouse progressive ankylosis gene, result in craniometaphyseal dysplasia. *Nat Genet*, **28**, 37-41.

3 Morava, E., Kuhnisch, J., Drijvers, J.M., Robben, J.H., Cremers, C., van Setten, P., Branten, A., Stumpp, S., de Jong, A., Voesenek, K. *et al.* (2011) Autosomal Recessive Mental Retardation, Deafness, Ankylosis, and Mild Hypophosphatemia Associated with a Novel ANKH Mutation in a Consanguineous Family. *J Clin Endocrinol Metab*.

4 Caswell, A., Guilland-Cumming, D.F., Hearn, P.R., McGuire, M.K. and Russell, R.G. (1983) Pathogenesis of chondrocalcinosis and pseudogout. Metabolism of inorganic pyrophosphate and production of calcium pyrophosphate dihydrate crystals. *Ann Rheum Dis*, **42 Suppl 1**, 27-37.

5 Kornak, U., Brancati, F., Le Merrer, M., Lichtenbelt, K., Hohne, W., Tinschert, S., Garaci, F.G., Dallapiccola, B. and Nurnberg, P. (2010) Three novel mutations in the ANK membrane protein cause craniometaphyseal dysplasia with variable conductive hearing loss. *Am J Med Genet A*, **152A**, 870-874.

6 Ho, A.M., Johnson, M.D. and Kingsley, D.M. (2000) Role of the mouse ank gene in control of tissue calcification and arthritis. *Science*, **289**, 265-270.

7 Sweet, H.O. and Green, M.C. (1981) Progressive ankylosis, a new skeletal mutation in the mouse. *J Hered*, **72**, 87-93.

8 Terkeltaub, R.A. (2001) Inorganic pyrophosphate generation and disposition in pathophysiology. *Am J Physiol Cell Physiol*, **281**, C1-C11.

9 Gurley, K.A., Reimer, R.J. and Kingsley, D.M. (2006) Biochemical and genetic analysis of ANK in arthritis and bone disease. *Am J Hum Genet*, **79**, 1017-1029.

10 Zhou, X., Cui, Y., Zhou, X. and Han, J. (2012) Phosphate/pyrophosphate and MV-related proteins in mineralisation: discoveries from mouse models. *Int J Biol Sci*, **8**, 778-790.

11 Williams, C.J. (2016) The role of ANKH in pathologic mineralization of cartilage. *Curr Opin Rheumatol*, **28**, 145-151.

12 Mitton-Fitzgerald, E., Gohr, C.M., Bettendorf, B. and Rosenthal, A.K. (2016) The Role of ANK in Calcium Pyrophosphate Deposition Disease. *Current rheumatology reports*, **18**, 25.

13 Fleisch, H., Russell, R.G. and Straumann, F. (1966) Effect of pyrophosphate on hydroxyapatite and its implications in calcium homeostasis. *Nature*, **212**, 901-903.

14 Wang, W., Xu, J., Du, B. and Kirsch, T. (2005) Role of the progressive ankylosis gene (ank) in cartilage mineralization. *Mol Cell Biol*, **25**, 312-323.

15 Yepes, M., Moore, E., Brown, S.A., Hanscom, H.N., Smith, E.P., Lawrence, D.A. and Winkles, J.A. (2003) Progressive ankylosis (Ank) protein is expressed by neurons and Ank immunohistochemical reactivity is increased by limbic seizures. *Laboratory investigation; a journal of technical methods and pathology*, **83**, 1025-1032.

16 Bonifacino, J.S. and Lippincott-Schwartz, J. (2003) Coat proteins: shaping membrane transport. *Nat Rev Mol Cell Biol*, **4**, 409-414.

17 Traub, L.M. (2009) Tickets to ride: selecting cargo for clathrin-regulated internalization. *Nat Rev Mol Cell Biol*, **10**, 583-596.

18 Bonifacino, J.S. and Traub, L.M. (2003) Signals for sorting of transmembrane proteins to endosomes and lysosomes. *Annu Rev Biochem*, **72**, 395-447.

19 Bonifacino, J.S. and Rojas, R. (2006) Retrograde transport from endosomes to the trans-Golgi network. *Nat Rev Mol Cell Biol*, **7**, 568-579.
20 Meyer, C., Zizioli, D., Lausmann, S., Eskelinen, E.L., Hamann, J., Saftig, P., von Figura, K. and Schu, P. (2000) mu1A-adaptin-deficient mice: lethality, loss of AP-1 binding and rerouting of mannose 6-phosphate receptors. *Embo J*, **19**, 2193-2203.
21 Crump, C.M., Xiang, Y., Thomas, L., Gu, F., Austin, C., Tooze, S.A. and Thomas, G. (2001) PACS-1 binding to adaptors is required for acidic cluster motif-mediated protein traffic. *Embo J*, **20**, 2191-2201.
22 Meyer, C., Eskelinen, E.L., Guruprasad, M.R., von Figura, K. and Schu, P. (2001) Mu 1A deficiency induces a profound increase in MPR300/IGF-II receptor internalization rate. *J Cell Sci*, **114**, 4469-4476.
23 Dinter, A. and Berger, E.G. (1998) Golgi-disturbing agents. *Histochem Cell Biol*, **109**, 571-590.
24 Minin, A.A. (1997) Dispersal of Golgi apparatus in nocodazole-treated fibroblasts is a kinesin-driven process. *J Cell Sci*, **110 (Pt 19)**, 2495-2505.
25 Puri, S., Bachert, C., Fimmel, C.J. and Linstedt, A.D. (2002) Cycling of early Golgi proteins via the cell surface and endosomes upon lumenal pH disruption. *Traffic*, **3**, 641-653.
26 Lippincott-Schwartz, J., Yuan, L., Tipper, C., Amherdt, M., Orci, L. and Klausner, R.D. (1991) Brefeldin A's effects on endosomes, lysosomes, and the TGN suggest a general mechanism for regulating organelle structure and membrane traffic. *Cell*, **67**, 601-616.
27 Zeghouf, M., Guibert, B., Zeeh, J.C. and Cherfils, J. (2005) Arf, Sec7 and Brefeldin A: a model towards the therapeutic inhibition of guanine nucleotide-exchange factors. *Biochem Soc Trans*, **33**, 1265-1268.
28 Preta, G., Cronin, J.G. and Sheldon, I.M. (2015) Dynasore - not just a dynamin inhibitor. *Cell communication and signaling : CCS*, **13**, 24.
29 Steinman, R.M., Mellman, I.S., Muller, W.A. and Cohn, Z.A. (1983) Endocytosis and the recycling of plasma membrane. *J Cell Biol*, **96**, 1-27.
30 De Matteis, M.A. and Luini, A. (2008) Exiting the Golgi complex. *Nat Rev Mol Cell Biol*, **9**, 273-284.
31 de Figueiredo, P., Polizotto, R.S., Drecktrah, D. and Brown, W.J. (1999) Membrane tubule-mediated reassembly and maintenance of the Golgi complex is disrupted by phospholipase A2 antagonists. *Mol Biol Cell*, **10**, 1763-1782.
32 Valente, C., Polishchuk, R. and De Matteis, M.A. (2010) Rab6 and myosin II at the cutting edge of membrane fission. *Nat Cell Biol*, **12**, 635-638.
33 Glyvuk, N., Tsytsyura, Y., Geumann, C., D'Hooge, R., Huve, J., Kratzke, M., Baltes, J., Boening, D., Klingauf, J. and Schu, P. (2010) AP-1/sigma1B-adaptin mediates endosomal synaptic vesicle recycling, learning and memory. *Embo J*, **29**, 1318-1330.
34 Leonard, D., Hayakawa, A., Lawe, D., Lambright, D., Bellve, K.D., Standley, C., Lifshitz, L.M., Fogarty, K.E. and Corvera, S. (2008) Sorting of EGF and transferrin at the plasma membrane and by cargo-specific signaling to EEA1-enriched endosomes. *J Cell Sci*, **121**, 3445-3458.
35 Cullen, P.J. (2008) Endosomal sorting and signalling: an emerging role for sorting nexins. *Nat Rev Mol Cell Biol*, **9**, 574-582.
36 Hoepfner, S., Severin, F., Cabezas, A., Habermann, B., Runge, A., Gillooly, D., Stenmark, H. and Zerial, M. (2005) Modulation of receptor recycling and degradation by the endosomal kinesin KIF16B. *Cell*, **121**, 437-450.
37 Jung, N., Wienisch, M., Gu, M., Rand, J.B., Muller, S.L., Krause, G., Jorgensen, E.M., Klingauf, J. and Haucke, V. (2007) Molecular basis of synaptic vesicle cargo recognition by the endocytic sorting adaptor stonin 2. *J Cell Biol*, **179**, 1497-1510.

38 Zobiack, N., Rescher, U., Ludwig, C., Zeuschner, D. and Gerke, V. (2003) The annexin 2/S100A10 complex controls the distribution of transferrin receptor-containing recycling endosomes. *Mol Biol Cell*, **14**, 4896-4908.
39 Cabezas, A., Bache, K.G., Brech, A. and Stenmark, H. (2005) Alix regulates cortical actin and the spatial distribution of endosomes. *J Cell Sci*, **118**, 2625-2635.
40 Shen, X., Xu, K.F., Fan, Q., Pacheco-Rodriguez, G., Moss, J. and Vaughan, M. (2006) Association of brefeldin A-inhibited guanine nucleotide-exchange protein 2 (BIG2) with recycling endosomes during transferrin uptake. *Proc Natl Acad Sci U S A*, **103**, 2635-2640.
41 Morel, E. and Gruenberg, J. (2009) Annexin A2 binding to endosomes and functions in endosomal transport are regulated by tyrosine 23 phosphorylation. *J Biol Chem*, **284**, 1604-1611.
42 Lee, I., Doray, B., Govero, J. and Kornfeld, S. (2008) Binding of cargo sorting signals to AP-1 enhances its association with ADP ribosylation factor 1-GTP. *J Cell Biol*, **180**, 467-472.
43 Kornak, U., Kasper, D., Bosl, M.R., Kaiser, E., Schweizer, M., Schulz, A., Friedrich, W., Delling, G. and Jentsch, T.J. (2001) Loss of the ClC-7 chloride channel leads to osteopetrosis in mice and man. *Cell*, **104**, 205-215.
44 Gunther, W., Luchow, A., Cluzeaud, F., Vandewalle, A. and Jentsch, T.J. (1998) ClC-5, the chloride channel mutated in Dent's disease, colocalizes with the proton pump in endocytotically active kidney cells. *Proc Natl Acad Sci U S A*, **95**, 8075-8080.
45 Mohammad-Panah, R., Wellhauser, L., Steinberg, B.E., Wang, Y., Huan, L.J., Liu, X.D. and Bear, C.E. (2009) An essential role for ClC-4 in transferrin receptor function revealed in studies of fibroblasts derived from Clcn4-null mice. *J Cell Sci*, **122**, 1229-1237.
46 Casey, J.R., Grinstein, S. and Orlowski, J. (2010) Sensors and regulators of intracellular pH. *Nat Rev Mol Cell Biol*, **11**, 50-61.
47 Cipriano, D.J., Wang, Y., Bond, S., Hinton, A., Jefferies, K.C., Qi, J. and Forgac, M. (2008) Structure and regulation of the vacuolar ATPases. *Biochim Biophys Acta*, **1777**, 599-604.
48 Brightman, A.O., Navas, P., Minnifield, N.M. and Morre, D.J. (1992) Pyrophosphate-induced acidification of trans cisternal elements of rat liver Golgi apparatus. *Biochim Biophys Acta*, **1104**, 188-194.
49 Maes, H., Kuchnio, A., Carmeliet, P. and Agostinis, P. (2014) How to teach an old dog new tricks: autophagy-independent action of chloroquine on the tumor vasculature. *Autophagy*, **10**, 2082-2084.
50 Dobrowolski, R., Vick, P., Ploper, D., Gumper, I., Snitkin, H., Sabatini, D.D. and De Robertis, E.M. (2012) Presenilin deficiency or lysosomal inhibition enhances Wnt signaling through relocalization of GSK3 to the late-endosomal compartment. *Cell reports*, **2**, 1316-1328.
51 Dunmore, B.J., Drake, K.M., Upton, P.D., Toshner, M.R., Aldred, M.A. and Morrell, N.W. (2013) The lysosomal inhibitor, chloroquine, increases cell surface BMPR-II levels and restores BMP9 signalling in endothelial cells harbouring BMPR-II mutations. *Hum Mol Genet*, **22**, 3667-3679.
52 Baron, R. and Kneissel, M. (2013) WNT signaling in bone homeostasis and disease: from human mutations to treatments. *Nat Med*, **19**, 179-192.
53 Einhorn, T.A. and Gerstenfeld, L.C. (2015) Fracture healing: mechanisms and interventions. *Nat Rev Rheumatol*, **11**, 45-54.
54 Cailotto, F., Sebillaud, S., Netter, P., Jouzeau, J.Y. and Bianchi, A. (2010) The inorganic pyrophosphate transporter ANK preserves the differentiated phenotype of articular chondrocyte. *J Biol Chem*, **285**, 10572-10582.

55 Thompson, R.J., Akana, H.C., Finnigan, C., Howell, K.E. and Caldwell, J.H. (2006) Anion channels transport ATP into the Golgi lumen. *Am J Physiol Cell Physiol*, **290**, C499-514.
56 Gu, G., Nars, M., Hentunen, T.A., Metsikko, K. and Vaananen, H.K. (2006) Isolated primary osteocytes express functional gap junctions in vitro. *Cell Tissue Res*, **323**, 263-271.
57 Campbell, C., Squicciarini, J., Shia, M., Pilch, P.F. and Fine, R.E. (1984) Identification of a protein kinase as an intrinsic component of rat liver coated vesicles. *Biochemistry*, **23**, 4420-4426.
58 Engqvist-Goldstein, A.E., Kessels, M.M., Chopra, V.S., Hayden, M.R. and Drubin, D.G. (1999) An actin-binding protein of the Sla2/Huntingtin interacting protein 1 family is a novel component of clathrin-coated pits and vesicles. *J Cell Biol*, **147**, 1503-1518.

Figure legends

Fig. 1. ANK localizes at the *trans*-Golgi and plasma membrane. (A) ANK was detected in human adult fibroblasts (HAF) with a specific ANK antibody (rabbit) targeting a C-terminal peptide. Different compartments of the secretory pathway ER to Golgi intermediate compartment, *cis*-Golgi (CGN), *trans*-Golgi (TGN), and cycling TGN were visualized by immunodetection of ERGIC-53, GM130, TGN46, and AP1-γ1 (γ-adaptin), respectively. Overlap of ANK localization (green) and the subcellular compartment marker (red) is indicated by yellow color. Subcellular localization is highlighted by insets and color intensity plots. Nuclei are demonstrated by DAPI staining (blue). **(B)** Overexpression of GFP-tagged ANK in HeLa cells showed perinuclear localization. Specificity of the ANK-GFP signal is indicated by absence of a green signal in a non-transfected cell (white asterisk). **(C)** Immunoblots of rat liver Golgi fractions showed enrichment of endogenous ANK and markers of the Golgi compartment (GS28 and AP1-γ1). ANK was detected with an ANK antibody (goat) kindly provided by Dr. Winkles. **(D)** Overexpression of pcDNA4_ANK in HeLa cells and subsequent immunostaining detected ANK at the Golgi apparatus (1) and at the plasma membrane (PM) (2) with further accumulation in PM ruffles (3). Z-stacks were generated by confocal microscopy. **(E)** Using cell surface biotinylation of HAFs (two independent cell lines), ANK was detected at the biotinylated PM (cell surface - CS) and in the biotinylation-inaccessible intracellular pool (cell lysate - CL). Successful biotinylation is indicated by transferrin receptor (TfR). **(F)** Protein preparations of purified calf clathrin-coated vesicles (CCV) were immunoblotted and analyzed for ANK expression. Endogenous ANK, CCV marker clathrin heavy chain (CHC), and α-adaptin were highly abundant. Ank was also present within crude CCV preparations from whole brain of control mice; while absence of signal in *ank/ank* mice confirms ANK antibody specificity. Scale bars indicate 20 μm.

Fig. 2. ANK sorting requires clathrin and its adaptors. (A) To test the impact of the ANK N- and C-terminus for intracellular sorting, TfR and CD8 alpha chain fusion proteins were cloned. The ANK N-terminus (M1-F76) was fused to extracellular domain of type 2 transmembrane protein TfR (N55-F760) and the ANK C-terminus (R453-E492) was fused to extracellular domain of type 1 transmembrane protein CD8 alpha chain (M1-C206). For detection both fusion proteins contained a N-terminal Xpress-tag. **(B)** Coexpression of ANK (red) and TfR-GFP (green) in HeLa cells resulted in strong overlap of both proteins. **(C)** Coexpression of TfR-GFP (green)/ANK-TfR (red) and TfR-GFP/CD8-ANK gained no overlap in HeLa cells. Western blot confirmed protein expression in HeLa cells. **(D)** Detection of endogenous Ank protein in murine μ1A-/- cells, lacking the μ-subunit of the AP1 complex, revealed cytosolic signals. In μ1A-/-:μ1A cells, having a rescue of the μ1A subunit, Ank showed strong perinuclear immunoreactivity. **(E)** Impact of clathrin-mediated transport for ANK subcellular sorting was analyzed upon siRNA ablation of the γ1-subunit of the adaptor protein complex 1 (protein AP1-γ1, gene AP1G1) and clathrin heavy chain (CHC). Both siRNAs disrupt localization of ANK to the Golgi. **(F)** Impact of the μ1-subunit of the adapter protein complex 2 (protein AP2-μ1, gene AP2M1) complex and PACS-1 on ANK subcellular localization was tested after siRNA treatment in HeLa cells. Ablation of both mRNAs diminished ANK localization to the Golgi. Scale bars indicate 20 μm.

Fig. 3. Impact of pharmacological intracellular transport blocking on ANK localization. (A) Treatment with the microtubule-depolymerizing drug nocodazole (5 μM, 60 min) in HeLa cells induced accumulation of ANK (green) in AP1-γ1 (red) positive Golgi mini-stacks.

Application of the cation ionophore Monensin A (10 µM, 60 min), blocking protein trafficking from medial to trans-Golgi, lead to partial overlap with AP1-γ1 (red) positive structures. Blocking anterograde protein transport from the ER with brefeldin A (BFA) (5 µg/ml, 60 min) caused partial accumulation of ANK in TGN46-positive (red) endosomes but not in ERGIC53 (red) structures. **(B)** Overexpression of ANK-GFP in HeLa cells showed strong overlap of ANK-GFP and TfR mainly in the perinuclear region. Incubation with dynasore (40 µM, 60 min), an inhibitor of dynamin mediated endocytosis, distributed the TfR throughout the cytoplasm. ANK remained localized within the perinuclear region. Incubation with chloroquine (200 µM, 60 min), an inhibitor of lysosomal acidification and endosome fusion, disproportionated TfR from the PM and the perinuclear region, while ANK accumulated at the PM and in perinuclear vesicular structures. White box indicates selected inset region. White arrows within the insets mark position of line scan generation. Line scans confirm accumulation of ANK upon chloroquine treatment. Scale bars indicate 20 µm.

Fig. 4. ANK regulates carrier formation at the TGN. (A) Golgi tubulation was induced by brief BFA (5 µg/ml, 5 min) treatment in HeLa cells. The Golgi compartment was subsequently immunostained and imaged with confocal microscopy identifying ANK (green) and TGN46 (red) within BFA induced Golgi tubules. **(B)** Golgi tubulation ability (5 µg/ml BFA, 5 min) was assessed in HeLa cells after knock-down with ANK siRNA#1 and subsequent immunostaining for RAB6 and TGN46. Confocal microscopy demonstrated reduced tubulation ability upon ANK knock-down. **(C)** Quantitative analysis of BFA induced Golgi tubules revealed diminished tubule length and number in ANK siRNA#1 treated HeLa cells. Cells were imaged with confocal microscopy and images were analyzed with AxioVision (Zeiss). For each condition tubules of >150 cells were measured. Statistical analysis was performed with unpaired t-test, ** $p \leq 0.01$. Error bars show SD. Scale bars indicate 20 µm.

Fig. 5. ANK regulates endosome function. (A) Cellular labelling of early endosomes was performed with transferrin (Tf, labelled with Alexa555, 5 µg/ml) for 6 min. In control HeLa cells Tf is distributed throughout the cytoplasm. HeLa cells treated with three independent siRNAs ANK#1-3 showed perinuclear accumulation of Tf (white arrow). **(B)** Counterstaining of internalized Tf (10 min) showed perinuclear enrichment of the early endosome antigen 1 (EEA1) marker in ANK#1 siRNA treated HeLa cells. Absence of ANK reduced EEA1 and Tf colocalization (inset). **(C)** Tf internalization was terminated after 2, 4, 5, and 10 min Tf incubation (5 µg/ml) by fixation and subsequent confocal imaging under identical exposure conditions. Image analysis (AxioVision) revealed a significant delay of Tf internalization in siRNAs ANK#1 treated HeLa cells at 6 and 10 min. For each time point and condition >300 cells were analyzed. **(D)** Tf recycling was performed after 30 min pre-incubation (Tf, labeled with Alexa555, 5 µg/ml) with subsequent chase for 5, 15, 30, and 60 min. Cells were fixed and imaged with confocal microscopy under identical exposure conditions. Tf recycling is at 15 min delayed in siRNAs ANK#1 treated HeLa cells. For each time point and condition ~100 cells were analyzed. **(E)** Tubule formation was induced with BFA (10 min, 5 µg/ml) to provoke ERC carrier formation. Control HeLa cells demonstrated tubule formation throughout the cytoplasm. In siRNAs ANK#1 HeLa cells the Tf labelled ERC had a perinuclear localization and show abundant tubule formation**. (F)** Relative distribution of TfR at the PM and non-acidic CCVs upon ANK ablation was assessed after transient transfection with pCI-TfR-pHluorin and subsequent imaging at pH 7.4, 5.5 and 10 (37). In siRNAs ANK#1 conditioned HeLa cells higher TfR levels were present at the PM with and without Tf stimulation. The amount of TfR in non-acidic CCVs was amplified under steady-state and

diminished upon Tf application. For each condition at steady-state ~100 cells and Tf treatment ~ 25 cells were analyzed. Statistical analysis was performed with unpaired t-test, * $p \leq 0.05$, ** $p \leq 0.01$. Error bars show SD. Scale bars indicate 20 µm.

Abbreviations

ANKH - human ankylosis gene, *Ank* - murine progressive ankylosis gene, ANK - human protein, Ank - murine protein, *ank/ank* - spontaneous loss-of-function mouse model, AP1 - clathrin adaptor-protein complex 1, AP1-γ1 - γ1-adaptin subunit of AP1 complex (protein AP1-γ1, gene *AP1G1*), AP2 - clathrin adaptor-protein complex 2, AP2-μ2 - μ2-subunit of the AP2 complex (protein AP2-μ2, gene *AP2M1*), BFA - brefeldin A, CCAL2 - familial chondrocalcinosis, CCV- clathrin-coated vesicles, CHC - clathrin heavy chain, CMD - craniometaphyseal dysplasia, ER - endoplasmic reticulum, MRDA - mental retardation, deafness, and ankylosis syndrome, TGN - trans-Golgi network, PACS-1 - phosphofurin acidic cluster sorting protein 1, PM - plasma membrane, PPi - pyrophosphate, Tf - transferrin, TfR - transferrin receptor, TGN46 - trans-Golgi network protein 46,

Figure 1

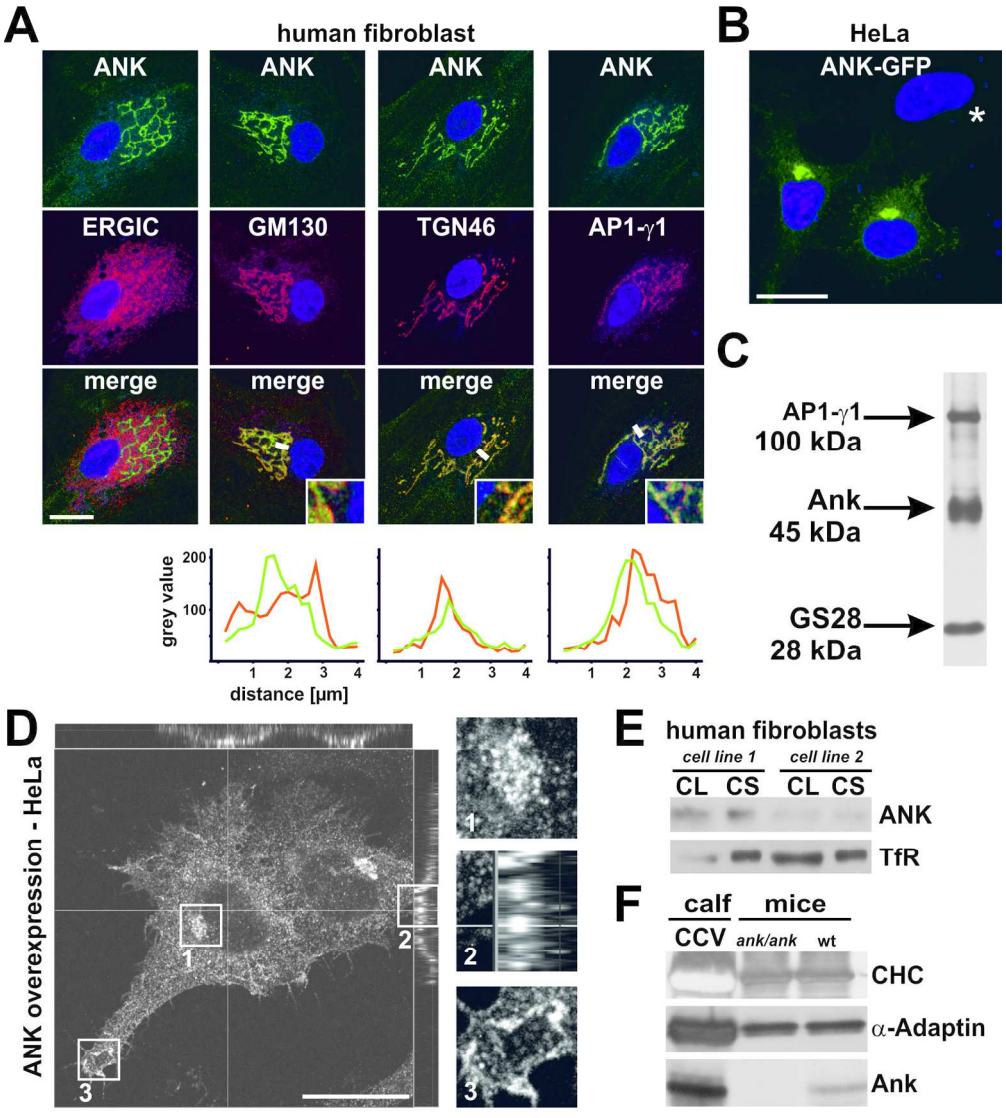

Figure 1

173x208mm (300 x 300 DPI)

Figure 2

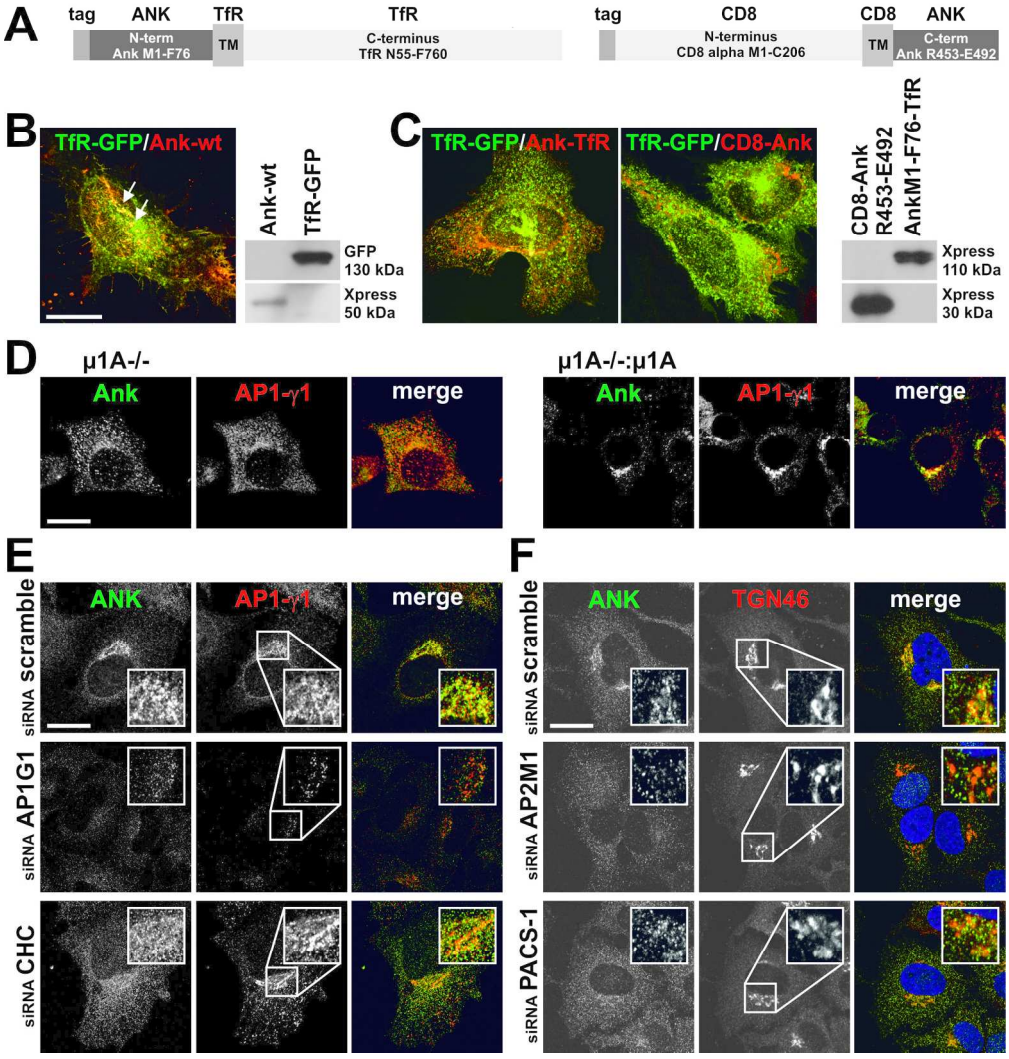

Figure 2

178x201mm (300 x 300 DPI)

Figure 3

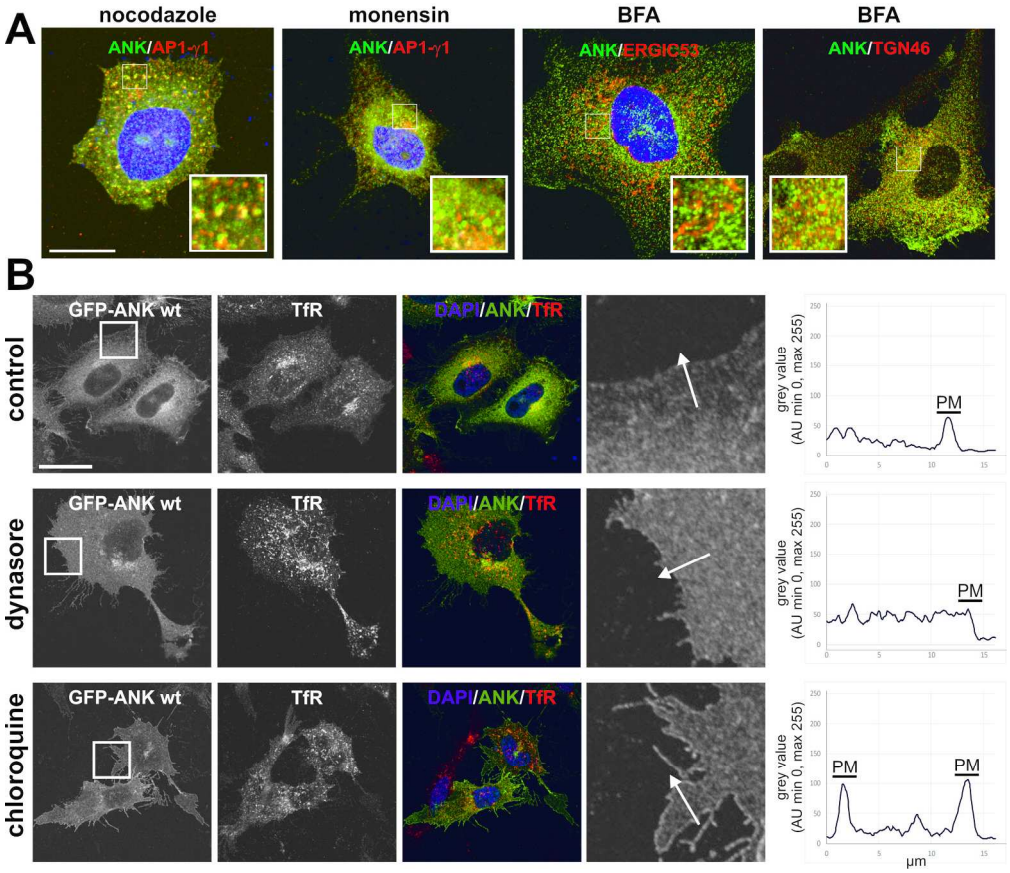

Figure 3

197x183mm (300 x 300 DPI)

Figure 4

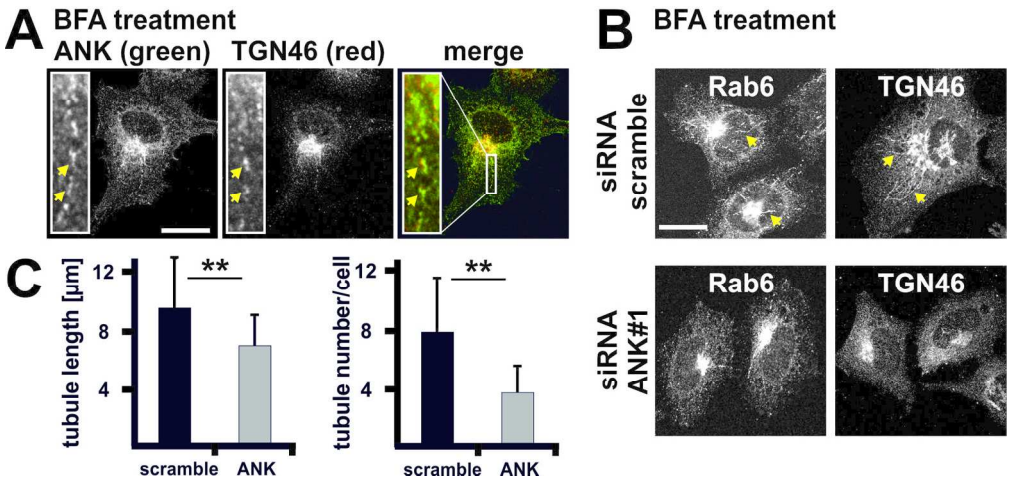

Figure 4

157x88mm (300 x 300 DPI)

Figure 5

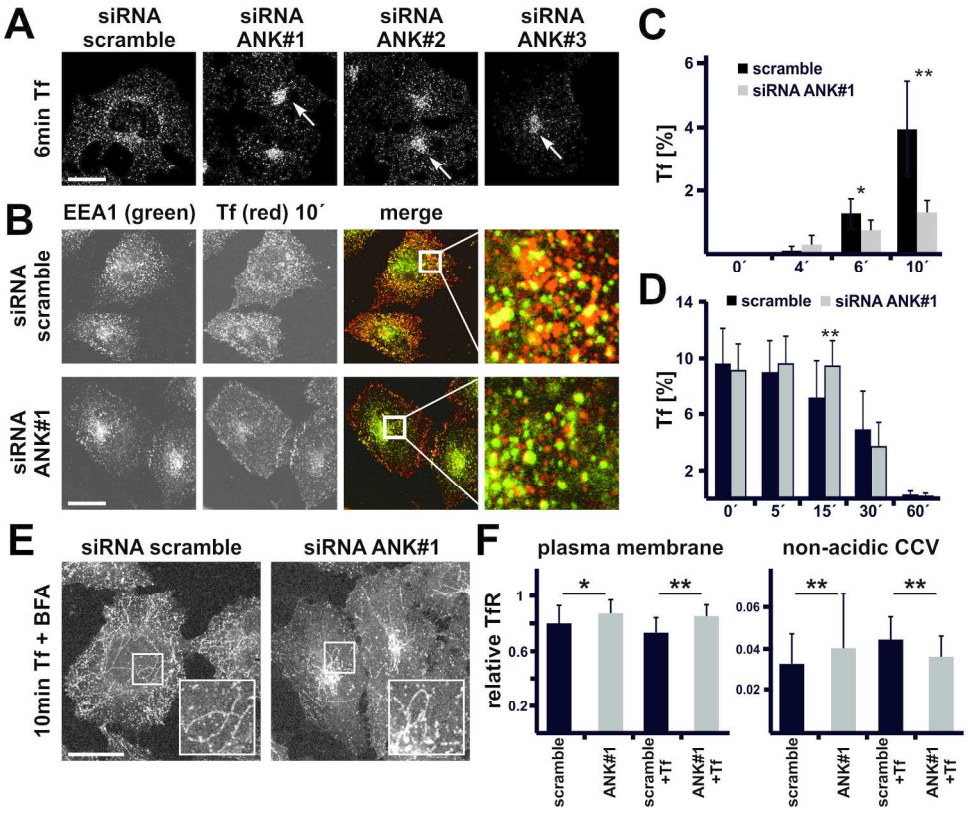

Figure 5

201x172mm (300 x 300 DPI)